Spring 2017

Pressure Dependence of Polycrystalline Magnesite and Dolomite

Cole Blasko
cb128@zips.uakron.edu

Pressure Dependence of Polycrystalline Magnesite and Dolomite

Cole Blasko

Department of Geology

Honors Research Project

Submitted to

The Honors College

Approved:

Date 26Apr17

Dr. Caleb Holyoke (signed)

Caleb W. Holyoke, III

Honors Project Sponsor (printed)

John Peck Date 4-26-17

Dr. John Peck (signed)

John Peck

Reader (printed)

Date 4/26/17

Dr. Meagan Ankney (signed)

Meagan Ankney

Reader (printed)

Accepted:

Date 4-26-17

Dr. Stephen Weeks (signed)

Steve Weeks

Department Head (printed)

John Peck Date 4-26-17

Dr. John Peck (signed)

John Peck

Honors Faculty Advisor (printed)

Date 4/26/2017

Dean, Honors College

Cole Blasko
Honors Research Project
Dr. Caleb Holyoke
The University of Akron Department of Geology
April 24th, 2017

Pressure Dependence of Polycrystalline Magnesite and Dolomite

ABSTRACT

Intermediate depth (170-400 km) deep focus earthquakes are observed in subducting slabs, but unlike shallow (50-170 km) and deep (400-660 km) deep focus earthquakes, the mechanism(s) responsible for them are not clear. Two common alteration products observed in peridotites, magnesite and dolomite, are stable along the pressure-temperature path of a subducting slab. Low pressure experiments indicate that these minerals are weaker than olivine, but there are no data about the pressure dependence of the strength of magnesite or dolomite. Magnesite and dolomite cylinders (1mm by 1mm) were deformed in stacked series to 25-30% strain using the deformation-DIA (DDIA) at Argonne National Lab at 500°C and three different pressures of 3.1 GPa, 5.8 GPa, and 6.2 GPa. In order to determine the pressure dependence of magnesite and dolomite deformed by low temperature plasticity, stacked samples allow direct observation of the materials' relative strengths via differences in strain rates. At all conditions, dolomite deformed at a constant strain rate, which does not evolve with increasing strain. However, magnesite strain weakened during all experiments. Magnesite is initially isoviscous or stronger than dolomite, but with increasing strain, became weaker than dolomite. These results indicate that presence of magnesite in subduction zones can cause strain localization and therefore be the likely source of intermediate depth deep focus earthquakes.

TABLE OF CONTENTS

1.0. INTRODUCTION

The responses of several key minerals to increasing pressures within a subduction zone can cause earthquakes at specific depths (Frohlich, 1989). Relatively shallow depth (50-170 km) deep focus earthquakes are likely caused by the dehydration of serpentine (Raleigh and Paterson, 1965; Raleigh, 1967) whereas deeper (400-670 km) deep focus earthquakes are likely caused by the phase transition of olivine to wadsleyite and ringwoodite (Kirby, 1987; Green and Burnley, 1989). Unlike the shallow and deep, deep focus earthquakes, intermediate depth deep focus earthquakes (170-400km) are not observed in all subducting slabs (Karato et al., 2001). Ductile instabilities in olivine have been proposed as a mechanism to cause these intermediate depth deep focus earthquakes (Griggs 1967; Karato et al., 2001; Kelemen and Hirth, 2007). However, not all slabs are made predominantly of olivine.

A possible source for intermediate depth, deep focus earthquakes is the presence of magnesian carbonates. Magnesite and dolomite are common alteration products of peridotite formed by reactions with carbonated fluids (Seto et al., 2008). These carbonate minerals are stable at the pressures (2-6 GPa) and temperatures (400-1000°C) of the mantle where intermediate depth deep focus earthquakes occur (Holyoke et al., 2014).

Although the source of intermediate depth (170-400 km) deep focus earthquakes is not entirely understood, low pressure experiments indicate magnesian carbonates are weaker than olivine and can, therefore, reduce the strength of the subducting slab leading to strain localization and possibly encourage seismicity (Holyoke et al., 2014). Holyoke et al. (2014) constructed a model of magnesite's strength using flow laws for all deformation mechanisms of the mineral. However, they did not determine the pressure dependence of the strength of magnesite and dolomite. We therefore performed experiments on magnesite and dolomite aggregate cores at

low temperature plasticity conditions that would be applicable to the intermediate depth deep focus earthquake region of a subducting slab.

2.0. METHODS

Pressure dependence experiments were conducted using the deformation-DIA (D-DIA) at beam-line 6 BMB at the Advanced Photon Source at Argonne National Laboratory in Lemont, Illinois. Under experimental conditions (T=500°C, P=3.1, 5.8, and 6.2GPa, $\dot{\varepsilon}$=2x10^{-5}/s), both magnesite and dolomite deformed by low temperature plasticity mechanisms. We stacked magnesite and dolomite cylinders to determine the relative strengths by visual inspection due to the differences in strain rate between the two samples at identical temperature and pressure conditions.

2.1. Sample description and assembly preparation

We used a natural fine-grained (d~1 μm) magnesite aggregate from Nevada (Figure 1A) and a fine-grained (d~1 μm) synthetic dolomite aggregate (Figure 1B) in all of the experiments of this study. These aggregates were also used by Holyoke et al. (2014) and Davis et al. (2010) to determine flow laws for magnesite and dolomite by low temperature plasticity mechanisms, respectively. Core cylinders measuring 1mm in diameter and 1mm in length of magnesite and synthetic dolomite were stacked in a graphite cylinder with rhenium and platinum foil between the samples and pistons (Figure 2). The graphite cylinder was inserted into a mullite sphere housed in a pyrophyllite cradle that formed a gasket between the six anvils of the D-DIA during compression (Durham et al., 2008). Changes in d-spacing of the lattice reflections were measured through the collection of X-ray spectra that allowed for pressure to be calculated (Wang et al., 2003; Raterron and Merkel, 2009). Space between the rhenium foils in radiographs

was measured and the time of measurements were recorded to calculate the strain and strain rate.

2.2. Experimental conditions

Magnesite and dolomite aggregate cores were deformed in series to 19-35% strain at 500° C and three different pressures of 3.1 GPa, 5.8 GPa, and 6.2 GPa (Table 1). Six pistons surrounding the sample assembly compressed the sample by means of oil pressure in three orthogonal orientations normal to faces of the sample assembly (Wang et al. 2003). Samples were first put under the desired pressure. Next, heat was applied by an electric current to a resistive, hollow graphite furnace that houses the samples. Applying a known voltage to the graphite cylinder furnace to bring it up to the desired temperature of 500° C. The desired temperature is achieved by utilizing calibrations showing a wattage that corresponds to a given temperature which is accurate to ±50°C. With the sample at known pressure and temperature conditions, hydrostatic data were collected using X-ray spectra. Data collection is achieved through multiple detectors recording energy dispersive diffraction patterns that have been generated from the synchrotron X-ray beam that have passed through the sample and the diamond anvil (Raterron et al., 2012). Uniaxial deformation was achieved by advancing two vertically positioned anvils at a constant rate. The D-DIA rams were advanced at a constant rate in all experiments (.003μm/sec), thus deforming the cylinders at ~$2x10^{-5}$/s. The rhenium foils in the load column (Figure 2) act as strain markers that allow sample length to be measured on the radiograph images to calculate strain and strain rate (Raterron et al., 2012).

2.3. Post deformation data collection

After reaching the desired strain, the voltage to the graphite furnace was shut off in order to quench the sample. The assembly was decompressed over a period of ~2 hours following quenching. Samples were impregnated with epoxy after their removal from the cell assembly.

After curing, the epoxy-encased sample was cut in half parallel to the direction of compression. The halves were impregnated once more with epoxy in order to fill in any void spaces that may have remained. The halves were then polished using a sequence of silicon carbide and aluminum oxide powders (600 grit, 1000 grit, 1200 grit, 3μm grit). The samples were analyzed using a scanning electron microscope (SEM) in secondary electron (SE) and back-scattered electron (BSE) modes to calculate grain size and observe microstructures and relative grain orientation.

3.0. RESULTS

Deformation of samples was performed at three different pressures of 3.1 GPa, 5.8 GPa, and 6.2 GPa for experiments Mag 005, Mag 006, and Mag 004, respectively (Table 1). All samples were deformed to high strains by ductile deformation mechanisms. Magnesite strain weakened over the course of deformation, while dolomite generally deformed at a constant strain rate throughout the experiment. Scanning electron microscope microstructural analysis indicates the microstructures are constant in both samples throughout the three experiments.

3.1. Low Pressure Experiment

At low pressure conditions (Mag 005: T=500°C, P=3.1 GPa, $\dot{\varepsilon}$=2x10^{-5}/s, σ=1.8 GPa) magnesite strain weakened when it reached a total strain of ε~5%. The strain rate in magnesite evolved from 2.9x10^{-5} /s to 2.0x10^{-4} /s (Figure 3A). In contrast, dolomite deformed at a constant strain rate of 1.1x10^{-4} /s for the duration of the experiment. Magnesite and dolomite were deformed until they reached a total strain of 27.23% and 35.58% respectively (Table 1). These results are consistent with flow law predictions. Stress on the load cell over time was highly variable due to the top and bottom rams of the D-DIA not advancing at the same rate. However, the general trend is an increase in stress over time (Figure 4A).

3.2. Intermediate Pressure Experiment

Magnesite and dolomite are initially isoviscous at the beginning of deformation at intermediate pressure conditions (Mag 006: T=500°C, P=5.8 GPa, $\dot{\varepsilon}$=2x10^{-5}/s, σ=1.8 GPa). At low strains of ε~2% magnesite began to strain weaken, and the strain rate evolved from 3.5x10^{-5} /s to 2.5x10^{-4} /s (Table 1). This strain weakening at intermediate pressures is the subtlest of the experiments in this study (Figure 3B). The higher strain rate remained relatively steady for the duration of the deformation experiment. The total strain of magnesite under these conditions reached 28.39% over ~4 hours of deformation. Throughout the experiment, dolomite deformed at a relatively constant strain rate of 5.9x10^{-5} /s to a total strain of 19.29%. Stresses acting on the load cell increased over time (Figure 4B). At intermediate pressures the increase in stress over time is the smallest.

3.3. High Pressure Experiment:

Magnesite and dolomite are nearly isoviscous at the high pressure conditions (Mag 004: T=500°C, P=6.2 GPa, $\dot{\varepsilon}$=2x10^{-5}/s, σ=2.9 GPa) (Figure 3C). Magnesite initially strained at a rate of 4.1x10^{-5} /s that evolved at a total strain of ε~4% to a rate of 1.7x10^{-4} /s (Table 1). Magnesite reached a total strain of 26.95% in this experiment. Contradictory to the flow law predictions of magnesite being stronger than dolomite at low pressures, dolomite reached a total strain of 25.20% during the experiment at a rate of 6.3x10^{-5} /s. Stress is again variable at the beginning of the experiment but eventually increases steadily over time (Figure 4C).

3.4. Microstructures

Stacking the samples allowed for direct observation of the relative strengths of the samples through differences in strain rate at these pressures, temperatures, and stresses. The magnesite sample shortened more than the dolomite sample (Figure 5) at T=500°C, P=5.8 GPa,

$\dot{\varepsilon}$=2x10^{-5}/s, σ=1.8 GPa. Magnesite grain size is unchanged (d~1 μm) after the experiment and grain shapes are still angular, but somewhat flattened (Figure 5B). Dolomite grain size is also unchanged, but the general shape of the grains is flattened perpendicular to the compression direction (Figure 5C). Microstructures in magnesite and dolomite are similar in all experiments.

4.0. DISCUSSION

4.1. Strain weakening and strength contrast

Magnesite strain weakened while dolomite deformed at a constant strain rate in all experiments. Magnesite strain weakening is not due to a transition in deformation mechanism. Considering the experimental conditions, deformation was likely caused by low temperature plasticity mechanisms. Although the exact mechanism is not clear, some minerals such as quartz and olivine strain weaken when deformed at high differential stresses (Hirth and Tullis, 1992). Quartz and olivine strain weaken as new fine grains form due to dynamic recrystallization. However, the grain size of the magnesite has not changed during these experiments leaving the source of strain weakening unclear.

At the start of each experiment magnesite is isoviscous or stronger than dolomite. Magnesite is stronger than dolomite in the lowest pressure experiment (Mag 005: T=500°C, P=3.1 GPa, $\dot{\varepsilon}$=2x10^{-5}/s, σ=1.8 GPa), but magnesite strain weakens at ε>5%. At total strains of 5-10% in all experiments there is an inversion of strength contrast where magnesite deformed much faster than dolomite (Figure 6). However, there is not a correlation between pressure and strength contrast (Figure 6).

4.2. Pressure dependence

The strength of fine-grained magnesite and dolomite increases as a function of increasing pressure (Figure 7). This result is consistent with other minerals, such as calcite (DeBresser, 2002), clinopyroxene (Amiguet et al., 2009), and olivine (Durham et al., 2009; Raterron et al., 2012). The results also indicate that the strength contrast between magnesian carbonates and olivine in the subducting slab may not be as great as previously reported by Holyoke et al. (2014). However, the pressure dependence (V*) of other mechanisms such as dislocation glide, dislocation creep, and diffusion creep that contribute to their model has not been determined. Through manipulation of flow law parameters, V* for magnesite was calculated to be 12.8×10^{-6} m^3/mol (Figure 7). The pressure dependence of magnesite and dolomite are not significantly different.

Deformation of subducting slabs at high pressures and temperatures caused by slab pull/ridge push may cause strain to localize in weaker phases in the subducting slabs. When comparing the strength of magnesite to the strength of other dominant mineral phases present in a subducting slab, such as serpentine and olivine, the strain weakening nature of fine-grained magnesite may lead to strain localization within these magnesite rich locations.

5.0. CONCLUSION

Uniaxial deformation experiments were performed on stacked polycrystalline magnesite and dolomite cores in the D-DIA deformation apparatus at 500°C and pressures of 3.1 GPa, 5.8 GPa, and 6.2 GPa. A synchrotron X-ray beam was utilized to produce energy spectra and radiographs that were used to calculate the pressure and strain, respectively, over time. Magnesite strain weakened in all experiments. Dolomite deformed at a constant strain rate at all

pressures. Magnesite is initially isoviscous or stronger than dolomite, but becomes weaker than dolomite with increasing strain. These results indicate that the strength of magnesite is sensitive to strain. If magnesite is present in subducting slabs composed dominantly of stronger olivine, strain may localize in magnesite rich zones and the strength contrast will continue to increase. This dynamic weakening could be a mechanism that causes intermediate depth deep focus earthquakes.

ACKNOWLEDGEMENTS

This study was supported by NSF grant EAR-1624240 to Dr. Caleb Holyoke, Dr. Paul Raterron, and Dr. Andreas Kronenberg. Thank you to The University of Akron Department of Geosciences and Dr. Caleb Holyoke, Dr. John Peck, and Dr. Meagan Ankney who helped in the writing of this paper. Special thanks to Dr. Paul Raterron, Leif Tokle, Nicholas Jackson, and Haiyan Chen who helped with experiments at the Advanced Photon Source beam line.

REFERENCES

Amiguet, E., Raterron, P., Cordier, P., Couvy, H., Chen, J., 2009. Deformation of diopside single crystal at mantle pressure. 1: Mechanical data. Physics of the Earth and Planetary Interiors 177, 122-129.

Davis, N.E., Kronenberg, A.K., Newman, J., 2008. Plasticity and diffusion creep of dolomite. Tectonophysics 456, 127-146.

De Bresser, J. H. P., 2002. On the mechanism of dislocation creep of calcite at high temperature: Inferences from experimentally measured pressure sensitivity and strain rate sensitivity of flow stress. Journal of Geophysical Research 107, 4-1 - 4-16.

Durham, W.B., Mei, S., Kohlstedt, D.L., Wang, L., Dixon, N.A., 2009. New measurements of activation volume in olivine under anhydrous conditions. Physics of the Earth and Planetary Interiors 172, 67-73.

Frohlich, C., 1989. The Nature of Deep-Focus Earthquakes. Annual Review of Earth and Planetary Sciences 17, 227-254.

Green, H.W., Burnley, P.C., 1989. A new self-organizing mechanism for deep-focus earthquakes. Letters to Nature 341, 733-737.

Griggs, D., 1967. Hydrolytic Weakening of Quartz and Other Silicates. Geophysics Journal Int. 14(1-4), 19-31.

Hirth, G., Tullis, J., 1992. Dislocation creep regimes in quartz aggregates. Journal of Structural Geology 14(2), 145-159.

Holyoke, C., Kronenberg A., Newman J., 2014. Microstructural evolution during strain localization in dolomite aggregates. Journal of Structural Geology 69, 449-464.

Holyoke, C., Kronenberg, A., Newman, J., 2013. Dislocation creep of polycrystalline dolomite. Tectonophysics 590, 72-82.

Holyoke, C., Kronenberg, A., Newman, J., Ulrich C., 2014. Rheology of magnesite. Journal of Geophysical Research: Solid Earth, 6534-6557.

Karato, S., Riedel, M.R., Yuen, D.A., 2001. Rheological structure and deformation of subducted slabs in the mantle transition zone: implications for mantle circulation and deep earthquakes. Physics of the Earth and Planetary Interiors 127, 83-108.

Kelemen, P., Hirth, G., 2007. A periodic shear-heating mechanism for intermediate-depth earthquakes in the mantle. Letters to Nature 446, 787-790.

Kirby, S., 1987. Localized polymorphic phase transformations in high-pressure faults and applications to the physical mechanism of deep earthquakes. Journal of Geophysical

Research 92, 13789-13800.

Raleigh, C., 1967. Tectonic Implications of Serpentinite Weakening. Geophysical Journal International 14, 113-118.

Raleigh, C.B., Paterson, M.S., 1965. Experimental deformation of serpentinite and its tectonic implications. Journal of Geophysical Research 70, 3965-3985.

Raterron, P., Girard, J., Chen, J., 2012. Activities of olivine slip systems in the upper mantle. Physics of the Earth and Planetary Interiors 200, 105-112.

Raterron, P., Merkel, S., 2009. In situ rheological measurements at extreme pressure and temperature using synchrotron X-ray diffraction and radiography. Journal of Synchrotron Radiation 16, 748-756.

Seto, Y., Hamane, D., Nagai, T., Fujino, K., 2008. Fate of carbonates within oceanic plates subducted to the lower mantle, and a possible mechanism of diamond formation. Physics and Chemistry of Minerals 35(4), 223-229.

Wang, Y., Durham, W., Getting, I., Weidner, D., 2003. The deformation-DIA: a new apparatus for high temperature triaxial deformation to pressures up to 15 GPa. Review of Scientific Instruments 74, 3002-3011.

Table 1. Summary of experimental results.

SAMPLE #	TEMP (C°)	PRESSURE (GPa)	STRESS (GPa)	GRAIN SIZE (μm)	STRAIN (%)	STRAIN RATES (/s)
Mag 005	500	3.1	1.8			
Magnesite				1	27.23	2.9E-05 to 2.0E-04
Dolomite				1	35.58	1.1E-04
Mag 006	500	5.8	1.8			
Magnesite				1	28.39	3.6E-05 to 2.5E-04
Dolomite				1	19.29	5.9E-05
Mag 004	500	6.2	2.9			
Magnesite				1	26.95	4.1E-05 to 1.7E-04
Dolomite				1	25.20	6.4E-05

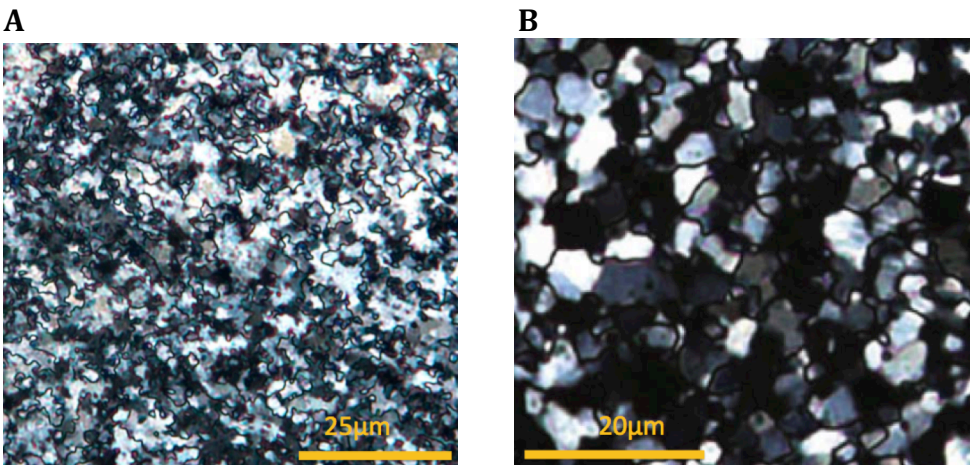

Figure 1. Both images are from an optical petrographic microscope with cross polarizers. Starting materials were fine-grained (d~1 µm) polycrystalline magnesite from Nevada (left) and a fine-grained (d~1 µm) synthetic dolomite aggregate (right). Both samples are relatively equigranular with virtually no pore space.

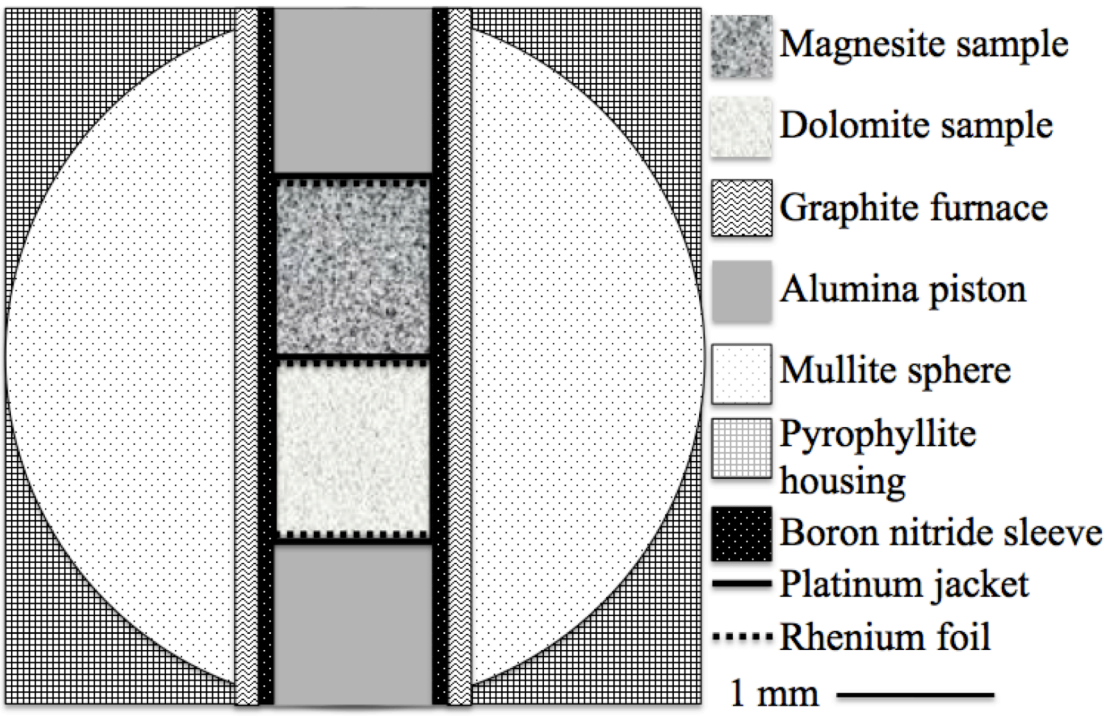

Figure 2. Cross section of cell assembly showing stacked samples between two alumina pistons with rhenium foil between each cylinder and a platinum jacket. Graphite furnace placed inside mullite sphere all housed within pyrophylllite cube.

A

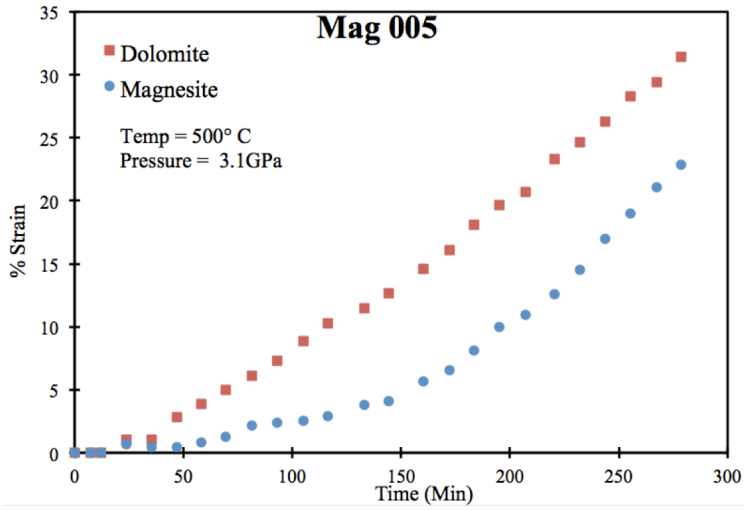

Figure 3. Plots of strain (%) vs. time (min) in order of increasing pressure.

(A) Magnesite strain weakened and would have become weaker than dolomite if curves are extrapolated to higher strains and the experiment was ran longer. Dolomite deforms at a constant strain rate throughout the experiment.

B

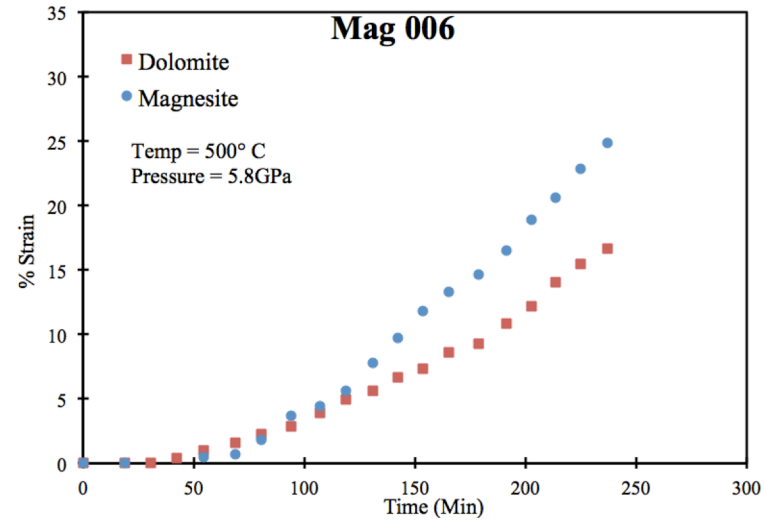

(B) Magnesite and dolomite are initially isoviscous but magnesite strain weakens and becomes much weaker than dolomite.

C

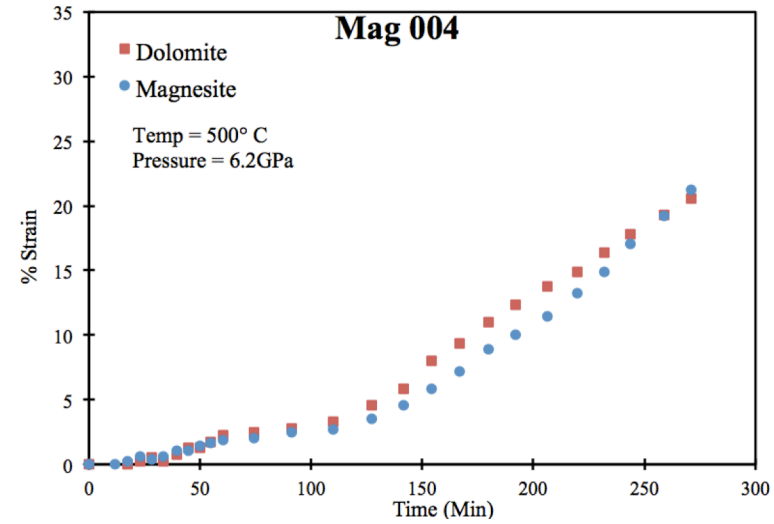

(C) Magnesite and dolomite are nearly isoviscous for the duration of the experiment. Magnesite strain weakens and becomes slightly weaker than dolomite at the end of the experiment. We believe the strength contrast would have increased further if the experiment went to higher strains.

A

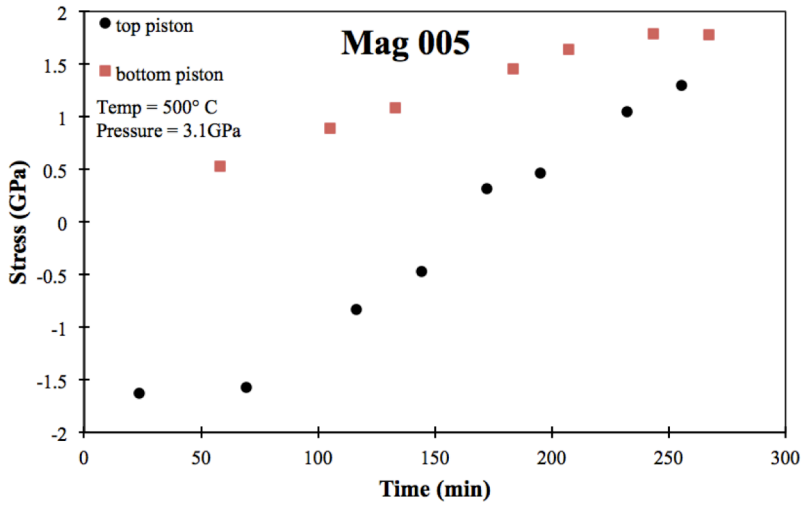

B

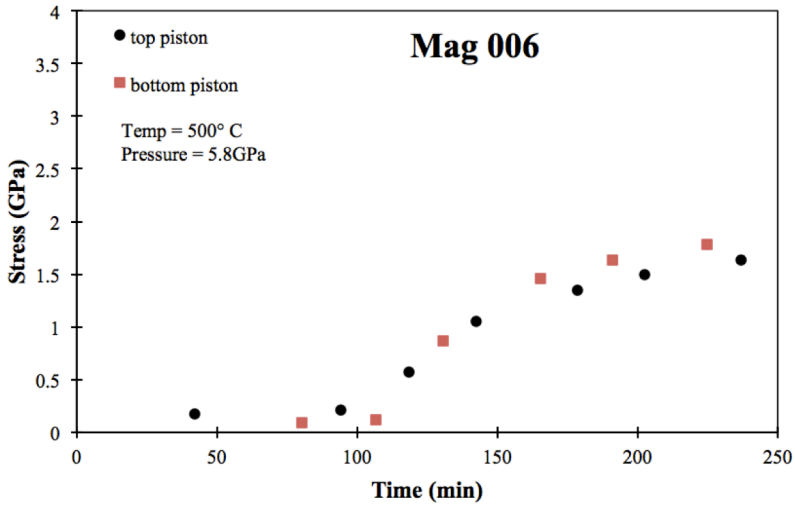

C

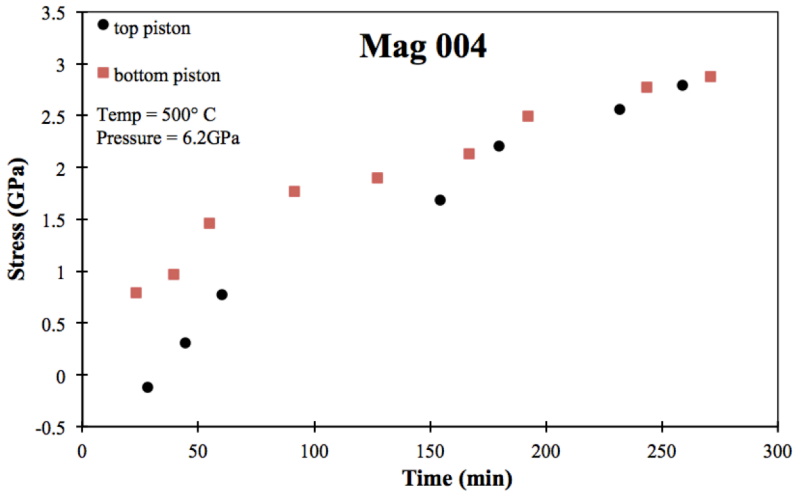

Figure 4. Plots of stress (GPa) vs. time (min) in order on increasing pressure.

(A) Stress is initially variable between the top and bottom piston but levels out over time reaching a maximum stress of 2.9 GPa

(B) Stress between the top and bottom piston is highly variable over time. However, the overall trend is increasing over time to reach a maximum stress of 1.8 GPa.

(C) Stress increases steadily over time reaching a maximum stress of 1.8 GPa.

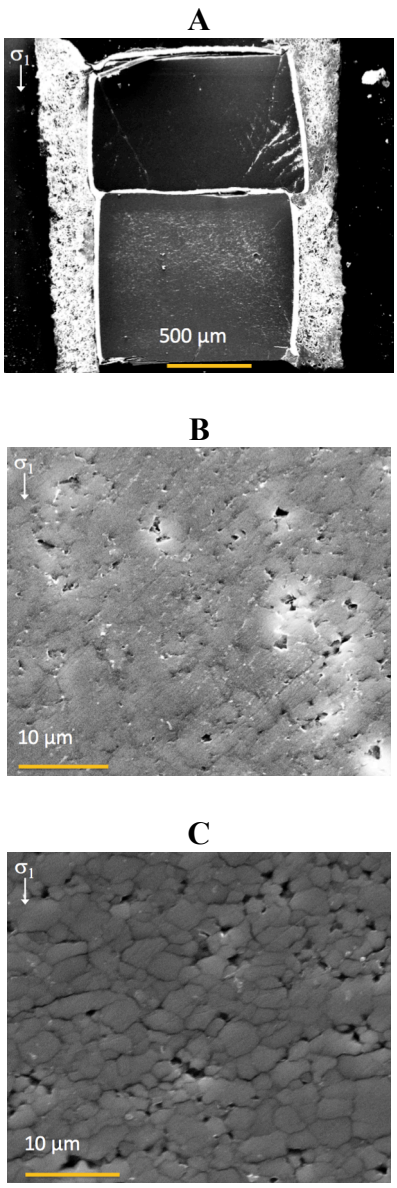

Figure 5. Post deformation SEM images of the microstructures of Mag 006 samples showing the whole assembly (A), magnesite grains (B), and dolomite grains (C), respectively.

(A) The upper cylinder (magnesite) shortened more than the lower cylinder (dolomite).
(B) Magnesite grains are angular and similar to the starting material.
(C) Dolomite grains are somewhat flattened perpendicular to the compression direction.

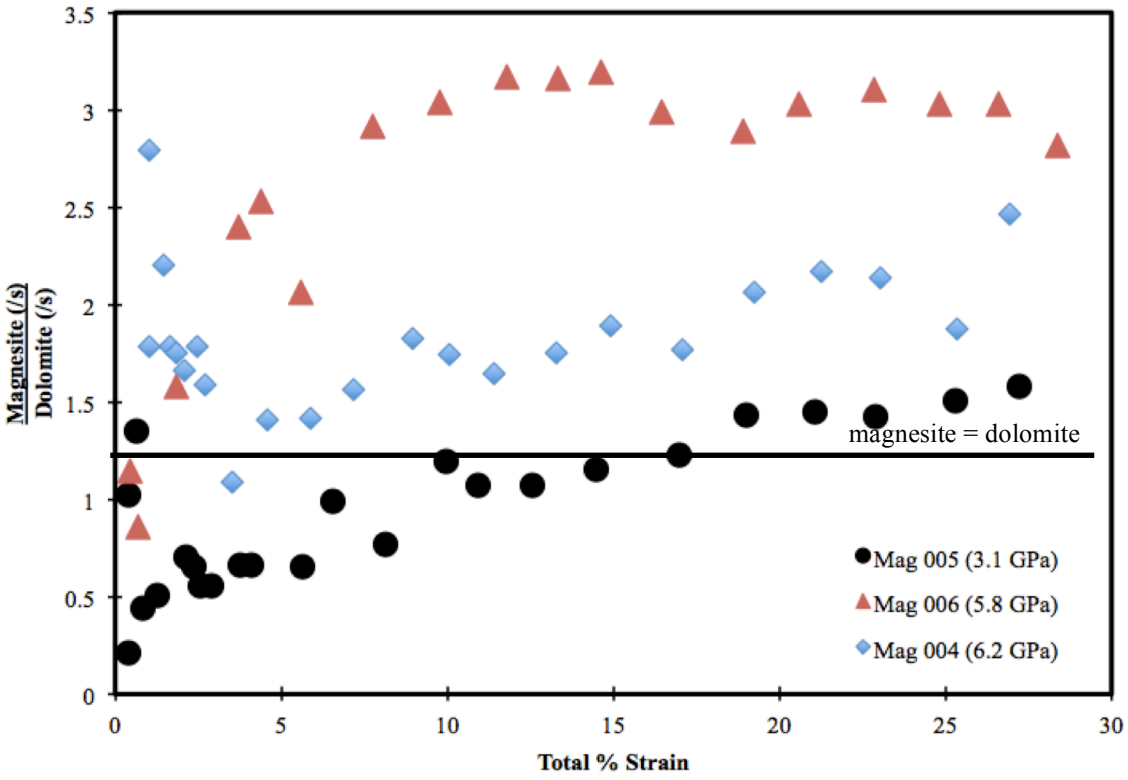

Figure 6. Plot showing the evolving strength contrast vs. the total strain (%). At a value of one, the strain rate of magnesite is equal to the strain rate of dolomite.

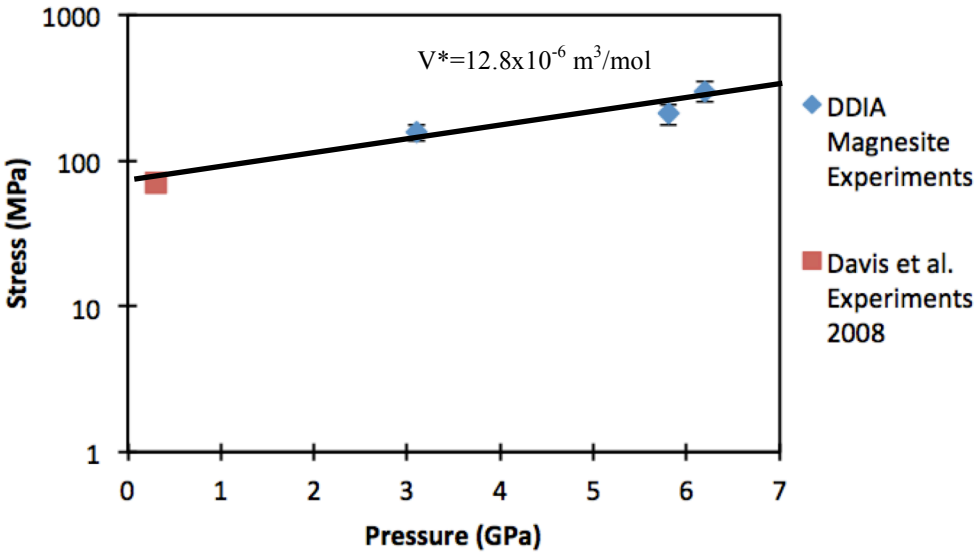

Figure 7. Strength of fine-grained magnesian carbonates as a function of increasing pressure. Three data points are from this experiment (blue symbol) and one point is from Davis et al. 2008 (red symbol).